Turkish Journal of Physics

http://journals.tubitak.gov.tr/physics/

Research Article

Turk J Phys
(2020) 44: 195 – 213
© TÜBİTAK
doi:10.3906/fiz-1907-27

Size-dependent electron chemical potential in nanostructures derived from statistical configuration

Desyana Olenka MARGARETTA, Nadya AMALIA, Fisca Dian UTAMI, Riri MURNIATI, Sparısoma VIRIDI, Mikrajuddin ABDULLAH*

Department of Physics, Bandung Institute of Technology, Bandung, Indonesia

Received: 31.07.2019 • **Accepted/Published Online:** 17.01.2020 • **Final Version:** 24.04.2020

Abstract: We rederived the fermion distribution function by considering the effect of assembly size. We did not use Stirling approximation to avoid the deviation generated by this approximation for a small number of constituents and small assembly size. Furthermore, we identified that in small systems, the chemical potential should also depend on the assembly size. We also rederived a general expression for the size-dependent chemical potential from a statistical configuration and showed that it is consistent with the results from previously reported theoretical or simulation methods. Finally, we applied the model to derive a size-dependent thermoelectric power factor of nanostructured materials. One important finding is that the power factor initially increases when reducing the particle size; however, it then reduces to approach zero when further reducing the material size, due to a dramatic change in the material behaviors.

Key words: Chemical potential, statistical configuration, thermoelectric power factor, nanostructure

1. Introduction

Chemical potential plays an essential role in materials physics since it controls several important properties. For example, thermoelectricity, the property of materials that are able to convert a temperature gradient into electric power, a potential approach for improvement of renewable energy resources [1, 2], depends on the chemical potential, where the thermoelectric power increases with the chemical potential [3–7]. Takeuchi et al. [3] showed that the fine electronic structure near the chemical potential plays an essential role in realizing unusual behavior in thermoelectric power [8–11]. Cook and Dickerson explained in a simple way how to understand the chemical potential, especially in small systems [12], starting from a definition of the chemical potential as $\mu = \partial U/\partial N]_{s,v}$, where U is the system internal energy, N is the number of particles in the system, S is the entropy, and V is the system volume. This relation states that the chemical potential is equal to the change in energy when one particle is added to the system while maintaining the entropy. Indeed, this is not the only relation to define the chemical potential.

Instead of the presence of a band gap such as that in the bulk state, in a nanostructure with a limited number of particles we only have a stack of discrete lines spreading in an energy range similar to the bandwidth. The distance between the discrete lines decreases as the particle size increases [13–17]. For small particle diameters, the energy spacing in the group is clearly separated [18]. For example, for a spherical particle that is assumed to have a spherical potential well, the energy of each discrete state is given by $\varepsilon_{n,\ell} = 2\hbar^2\chi_{n\ell}^2/m_e^*D^2$, where n and ℓ are quantum numbers, $\hbar$ is Planck's constant, $\chi_{n\ell}$ is the root of a Bessel function, m_e^* is the

*Correspondence: mikrajuddin@gmail.com

effective mass of the electron or the hole, and D is the particle diameter [15, 16]. It is clear that if a particle is added to the system (electron or hole), to maintain the entropy, the system energy must be reduced by at least $-\Delta\varepsilon_{n,\ell} \propto -1/D^2$. Therefore, we can conclude that the chemical potential will depend on the particle size as $\Delta\mu(D) \propto 1/D^2$.

There are many reports that the chemical potential of nanostructures depends on the size. Champbell and Mao proposed an increment of chemical potential relative to that for an infinitely large particle as $\Delta\mu(D) = [(3\gamma_m - E_{adh})(1+D_0/D)(2v_m/D)$, where γ_m is the surface energy of the bulk metal, E_{adh} is the adhesion energy of the bulk metal/oxide interface, v_m is the molar volume of the bulk metal, and D_0 is a constant ($\approx$1.5 nm for a transition metal) [19]. The equation was compared to data of Cu on $CeO_{1.96}(111)$, Ag on $CeO_{1.96}(111)$, Au on $CeO_{1.96}(111)$, Ag on $Fe_3O_4(111)$, and Ag on MgO(100). From this equation, the chemical potential can be written as $\mu(D) = \mu(\infty) + \Delta\mu(D)$.

Nagaev provided a compressive review of the size dependence of the chemical potential [20]. For example, an increase in the chemical potential dependence on the particle size is approximated as $\Delta\mu \propto \gamma A/N$, where A is the surface area. From this we obtain $\Delta\mu = \kappa v_m \gamma/D$ where κ is a constant. This equation is similar to that previously proposed [21]. Simulation by Croitoru et al. showed that for small nanoparticles, the chemical potential can be approximated by $\mu(D) = \mu(\infty) + 2\hbar/m_e^* \alpha_{i\ell}^2 D^2$ [18], with $\alpha_{i\ell}$ the ith zero of a spherical Bessel function of the first kind, $\mathrm{j}_l(x)$.

Kiyonaga et al. reported an increase in the Fermi energy in TiO_2-supported Au particles of sizes ranging between 3.0 and 13 nm, where the Fermi energy increased with diameter [22]. In addition, there have been several theoretical works and simulations regarding the dependence of the Fermi energy or chemical potential on size [23–26]. For example, Sodha and Dubey [24] applied the potential equation from Seitz [27] for a thin film of thickness d deposited on a dielectric substrate as a potential well and obtained an equation relating the Fermi energy with the film thickness in a complicated form [24]. They also derived an equation for spherical particles and obtained the same complicated relation for the Fermi energy and the particle diameter.

Sieperman also derived equations explaining the dependence of the excess chemical potential on the number of particles forming an assembly [26]. Korotun theoretically showed that the Fermi energy of Al and Au nanoparticles increases with decreasing particle diameter, although the increases are not continuous, and on average, the dependence satisfies the empirical function $\varepsilon_F(D) = \varepsilon_F(\infty)(1 + p/D^\delta)$, where p and δ are positive constants and $\varepsilon_F(\infty)$ is the Fermi energy in the bulk state [28]. Using a simple quantum well model, Seki also showed that the chemical potential of an electron in a thin slab depends on the slab thickness [29].

From all those reports arise the following questions: How can we prove fundamentally that the chemical potential depends on the assembly size? Can we show from a derivation of the distribution function that the fermion chemical potential depends on the assembly size? The purpose of this work is to show from the initial consideration, i.e. from the derivation of the distribution function, that the fermion chemical potential depends on the assembly size as well as the size dependence of the thermoelectric power factor.

In this work, we rederive the distribution functions for an assembly consisting of an arbitrary particle number, including very small particle numbers. We will derive the distribution function for fermion assemblies using a method similar to that discussed by Turoff [30]. Using this approach, we are free to apply the method for arbitrary assembly sizes (arbitrary number of particles).

2. Theoretical derivation

2.1. The dependence of the distribution function on the assembly size

We consider an assembly consisting of N identical noninteracting fermions with volume V and temperature T, with the energies of the assembly divided into groups. Each group has a large number of discrete states. However, although a group consists of a large number of states, we further consider that the ith group has an average energy ε_i and a number of states g_i and is occupied by n_i particles, as illustrated in Figure 1. As explained in standard statistical physics books [31–33], the number of different ways of arranging the fermions into all the groups in Figure 1a is

$$W = \prod_s \frac{g_s!}{n_s!(g_s - n_s)!}. \tag{1}$$

If an incremental external energy dU is supplied to the assembly, it results in one particle from a state in the pth group jumping to a state in the qth group (Figure 1b). The energy in the pth group is ε_p, and the energy in the qth group is ε_q. Hence, the energy increment satisfies $dU = \varepsilon_q - \varepsilon_p$. This jumping causes the number of particles in the pth (qth) group to change to $n_p - 1(n_q + 1)$, so by referring to Equation (1), the number of different ways of arranging the particles into new configurations (Figure 1b) becomes [30, 41]

$$W = \left(\prod_s \frac{g_s!}{n_s!(g_s - n_s)!}\right)\left(\frac{n_p}{g_p - n_p + 1}\frac{g_q - n_p}{n_q + 1}\right)$$

$$= W\left(\frac{n_p}{g - n_p + 1}\frac{g - n_q}{n_q + 1}\right). \tag{2}$$

We assume that even the number of particles forming the assembly is finite, and the following condition is always fulfilled: $n_p, n_q >> 1$. Based on this condition, Equation (2) can be approximated as

$$W' \approx W\left(\frac{n_p}{g_p - n_p}\frac{g_q - n_q}{n_q}\right). \tag{3}$$

We then use the definition of entropy as $S = klnW$ and $S' = klnW'$. The change in entropy due to a particle jumping is $dS = S' - S$. Based on this definition, Equation (3) becomes

$$dS \approx kln\left(\frac{n_p}{g_p - n_p}\frac{g_q - n_q}{n_q}\right). \tag{4}$$

We have a thermodynamic equation relating the energy, entropy, and temperature as $T = \partial U/\partial S$ or $dU \approx TdS$. If this definition is applied to Equation (4), we obtain

$$\varepsilon_q - \varepsilon_p \approx kTln\left(\frac{n_p}{g_p - n_p}\frac{g_q - n_q}{n_q}\right), \tag{5}$$

which can be rearranged as

$$\frac{n_p/(g_p - n_p)}{n_q/(g_q - n_q)} = \frac{exp(-\varepsilon_p/kT)}{exp(-\varepsilon_q/kT)}. \tag{6}$$

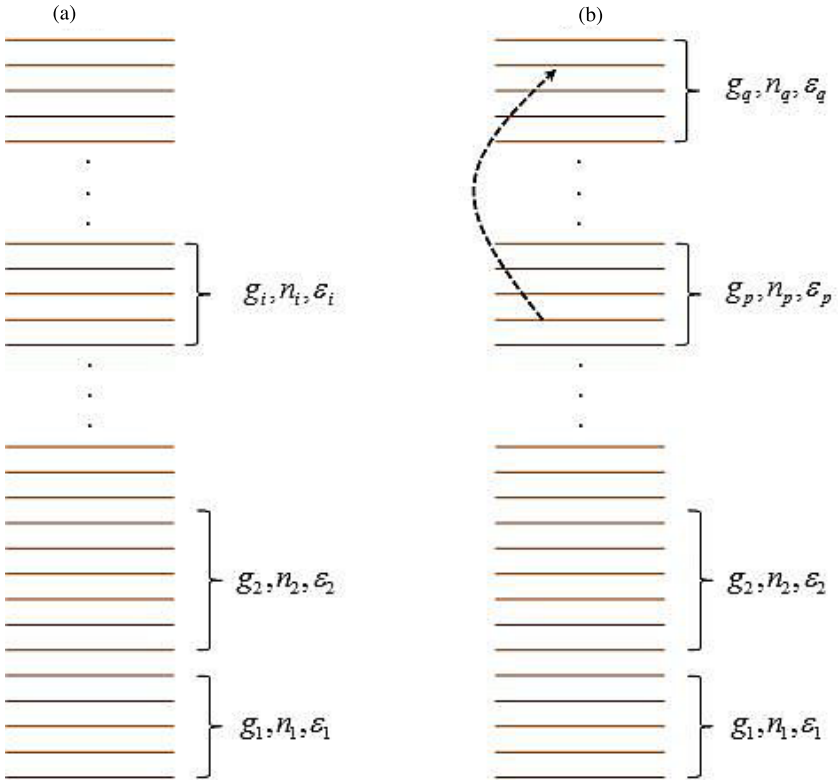

Figure 1. (a) The energies of the particles forming the assembly are assumed to be discrete, and several nearest energies are grouped. The sth group has g_s states and an average energy of g_s, and it is occupied by ns particles. (b) One particle in a state in the pth group jumps to a state in the qth group, implying that the number of particles in the pth group decreases by one while the number of particles in the qth group increases by one.

From Equation (6), we obtain the general expression

$$\frac{n_s}{g_s - n_s} = \psi(V,T)e^{-\varepsilon_s/kT}, \tag{7}$$

where ψ depends only on constant parameters belonging to the assembly. In equilibrium, the constant parameters are temperature and volume.

Let us define $\psi(V,T) = e^{\mu(V,T)/kT}$. Based on this definition, the dependence of the number of particles in the sth group on the number of states in the same group can be expressed as

$$n_s = \frac{g_s}{e^{(\varepsilon_s - \mu(V,T))/kT} + 1}. \tag{8}$$

Equation (8) describes the dependence of the distribution function on the assembly size merely because of the dependence of the chemical potential on size. The form of the distribution function itself does not change.

2.2. General formula for the size dependence of the chemical potential

The dependence of the chemical potential on particle size can also be derived statistically as follows. If one additional fermion is added to the system, the configuration in Equation (1) will change. To maintain the

entropy, the number of fermions in each group must reorganize. Some groups will lose fermions, and other groups will receive new fermions. Suppose the change in the number of fermions in the sth group is δn_s, which might be a positive or negative integer or zero and satisfies $|\delta n_s| << n_2$. The new number of configurations becomes

$$W^+ = \prod_s \frac{g_s!}{(n_s+\delta n_s)!(g_s-n_s-\delta n_s)!}$$

$$= \prod_s \frac{g_s!}{n_s!(g_s-n_s)!} \frac{(g_s-n_s-\delta_s+1)...(g_s-n_s)}{(n_s+1)...(n_s+\delta n_s)}$$

$$= W \prod_s \frac{(g_s-n_s-\delta_s+1)...(g_s-n_s)}{(n_s+1)...(n_s+\delta n_s)}. \tag{9}$$

Since $S = klnW$ and $S^+ = klnW^+$, to conserve entropy, the following equality must be satisfied:

$$\prod_s \frac{(g_s-n_s-\delta_s+1)...(g_s-n_s)}{(n_s+1)...(n_s+\delta n_s)} = \prod_s \prod_k \frac{(g_s-n_s-\delta_s+k)}{(n_s+k)} = 1. \tag{10}$$

The equality is thoroughly satisfied if

$$\frac{(g_s-n_s-\delta n_s+k)}{(n_s+k)} = 1 \tag{11}$$

for all k. From Equation. (11), we have $g_s - n_s - \delta n_s + k = n_s + k$, resulting in

$$\delta_s = g_s - 2n_s. \tag{12}$$

The change in energy when the entropy is constant is simply the chemical potential. Therefore, the chemical potential in the present case is

$$\mu = \sum_s \varepsilon_s \delta n_s$$

$$= \sum_s \varepsilon_s (g_s - 2n_s)$$

$$= \sum_s \varepsilon_s g_s - 2\sum_s n_s \varepsilon_s$$

$$= \sum_s \varepsilon_s g_s - \langle 2\varepsilon \rangle, \tag{13}$$

where $\langle \varepsilon \rangle$ is the average specific energy.

The energy of each group should be multiplied by the energy spacing between the discrete states. For a confined system, this is proportional to the inverse of the particle diameter power and some positive value. We can then approximate

$$\varepsilon_s = \frac{\theta_s}{D^\sigma}, \tag{14}$$

where θ_s is real and σ is a positive number. In most cases, $\sigma = 2$ [34–40].

The average energy depends on the particle size. We can estimate the average energy based on data of the specific heat capacity. Since the heat capacity is $C_v = d\langle\varepsilon\rangle/dT$, we can assume that the dependence of the specific energy on the particle dimension is precisely the same as the dependence of the heat capacity on the dimension. There are many proposals for the dependence of heat capacity on particle size, such as those by Singh et al. [41] and Patel et al. [42], $C_v(D) = \dfrac{C_v(\infty)}{1-\xi/D}$, where $C_v(\infty)$ is the specific heat capacity in the bulk state and ξ is a constant. Zhang et al. proposed $C_v(D) = C_v(\infty)[1 - 1/(D/D_0 - 1)]$ to explain the size dependence of the melting temperature, where D_0 is a constant [43]. Meanwhile, Xiong et al. proposed $C_v = 9R(T/\Theta_D)^3 \int_0^{\Theta_D/T} x^4 e^x (e^x - 1)^{-2} dx$, with R being the gas constant, and the Debye temperature satisfies $\Theta_D(D) = \Theta_D(\infty)(1 - \theta/D)$, where $\Theta_D(\infty)$ is the Debye temperature in the bulk state and θ is a constant [44]. The electronic heat capacity of metals satisfies $C_v = bT$, where T is temperature and b is a factor independent of temperature [33]. Therefore, for nanometer-sized materials, the heat capacity has the relation $C_v(D) = b(D)T$, and the average energy is given by $\langle\varepsilon\rangle = \int C_v dT = \frac{1}{2}C_v T^2 + const$, showing that the size dependence of the average energy is similar to that of the heat capacity. Using the aforementioned arguments, we can approximate

$$\mu(D) = \frac{\sum_s \varepsilon_s \theta_s}{D^\sigma} - A\phi(D), \tag{15}$$

with $\phi(D)$ being a function of D, based on Singh et al. [41], Zhang et al. [43], Xiong et al.[44], or others. In each case, it always satisfies $\phi(\infty) = 1$. A further approximation is found by considering $\sum_s \varepsilon_s \theta_s \approx C$ as a constant. Therefore, we obtain the following approximate expression:

$$\mu(D) \approx \frac{C}{D^\sigma} - A\phi(D). \tag{16}$$

In the case of $D \to \sigma$, we have $\mu(\infty) \approx -A$. Consequently, Eq. (16) can be further explicitly expressed as

$$\begin{aligned} \mu(D) &\approx \frac{C}{D^\sigma} + \mu(\infty)\phi(D) \\ &\approx \mu(\infty)\left(\phi(D) + \frac{C'}{D^\sigma}\right), \end{aligned} \tag{17}$$

with $C' = C/\mu(\infty)$

Equation (17) is the general equation for the size dependence of the chemical potential. Different materials might have slightly different forms such as different σ or a different function $\phi(D)$. However, they must still

satisfy $\phi(\infty) = 1$, and σ should not be far from 2. In general, Equation (17) states that the chemical potential increases or decreases as the size decreases, depending on the function $\phi(D)$. How far it increases depends on the function $\phi(D)$, which originates from the material properties and the effect of the surrounding material.

3. Discussion

3.1. Some proofs of size-dependent chemical potential

Now let us show that Equation (17) can explain several observations of the size dependence of the chemical potential, as mentioned in the Introduction. The chemical potential proposed by Campbell and Mao [19], which can be written as

$$\mu(D) = \mu(\infty)\left[1 + \frac{2v_m(3\gamma_m - E_{adh})/\mu(\infty)}{D} + \frac{2v_m(3\gamma_m - E_{edh})D_0/\mu(\infty)}{D^2}\right], \tag{18}$$

satisfies Equation (17) when selecting $\sigma = 2$, $C' = 2v_m(3\gamma_m - E_{adh})D_0/\mu(\infty)$, and $\phi(D) = 1 + (2v_m(3\gamma_m - E_{adh})/\mu(\infty))/D$. It is clear here that $\phi(\infty) \to 1$, as expected. The chemical potential proposed by Nagaev [20] as

$$\mu(D) = \mu(\infty)\left[1 + \frac{\kappa v_m\gamma/\mu(\infty)}{D}\right] \tag{19}$$

can be considered as Equation (17) when choosing $C = 0$ and $\phi(D) = 1 + (\kappa v_m\gamma/\mu(\infty))/D$ or $\sigma = 1$, $C' = \kappa v_m\gamma/\mu(\infty)$ and $\phi(D) = 1$. The chemical potential simulated by Croitoru et al. [18]that can be expressed as

$$\mu(D) = \mu(\infty)\left[1 + \frac{2\hbar^2/m_e\alpha_{il}^2\mu(\infty)}{D^2}\right] \tag{20}$$

is consistent with Equation (17) when choosing $\sigma = 2, C' = (2\hbar^2/m_e\mu(\infty))\alpha_{il}^2$, and $\phi(D) = 1$. The chemical potential proposed by Seki [29] can be rewritten as

$$\mu(L) \approx \mu(\infty)\left[1 + \frac{a}{L} + \frac{b}{L^2}\right]^2 \tag{21}$$

with

$$\mu(\infty) \approx \frac{h^2}{2m}\left(\frac{9\pi}{4}\right)^{1/3}\frac{1}{r_s},$$

$$a \approx \left(\frac{4}{9\pi}\right)^{1/3}\frac{\pi r_s}{4},$$

$$b \approx \frac{7\pi^{5/3}r_s^2}{63}\left(\frac{4}{9\pi}\right)^{1/3}.$$

Furthermore, Equation (21) can be expanded as

$$\mu(\infty) \approx \mu(\infty)\left[1 + \frac{2a}{L} + \frac{a^2 + 2b}{L^2} + \frac{2ab}{L^3} + \frac{b^2}{L^4}\right], \tag{22}$$

which also satisfies Equation (17) when choosing $\sigma = 2, C' = a^2 + 2b$, and $\phi(L) = 1 + 2a/L + 2ab/L^3 + b^2/L^4$. The chemical potential in an intrinsic semiconductor can be written as [45]

$$\mu = \frac{1}{2}E_g + \frac{3}{4}kTln\left(\frac{m_k^*}{m_e^*}\right), \tag{23}$$

where m_k^* is the effective mass of the hole. However, the band gap of a semiconductor has been known to depend on size, as proposed by Brus [46]:

$$E_g(D) = E_g(\infty) + \frac{2\hbar^2\pi^2}{m_{eff}D^2} - \frac{3.57e^2}{\varepsilon D}, \tag{24}$$

where m_{eff} is the reduced mass and ε is the dielectric constant of the nanoparticles. Using a finite-depth square-well effective mass approximation to provide a quantitative description of the quantum confinement effect, Ferreira et al. obtained a new analytical expression for the size dependence of colloidal semiconductor nanocrystals as [47]

$$E_g(D) = E_g(\infty) + \frac{2\hbar^2\pi^2}{m_{eff}D^2} - \frac{3.57e^2}{\varepsilon D} + \frac{\beta e^2}{\varepsilon D}. \tag{25}$$

Based on tight-binding molecular dynamic simulations, Takai et al. [48] confirmed that the band gap of Si, 3C-SiC, and C quantum dots can be fitted with

$$E_g(D) = E_g(\infty) + \frac{a}{D^2}$$

or

$$E_g(D) = E_g(\infty) + \frac{a'}{D^2} + \frac{b'}{D}, \tag{26}$$

with $(Eg(\infty), a, a, b)$ being (1.17 eV, 4.83 eV nm^2, 3.13 eV nm^2, 0.576 Ev nm), (2.40 eV, 3.29 eV nm^2, 2.24 eV nm^2, 0.453 Ev nm), and (5.50 eV, 4.11 eV nm^2, 2.34 eV nm^2, 0.910 Ev nm) for S, SiC, and C, respectively. In other reports, the band gap of most semiconductors satisfies the approximate formula

$$E_g(L) \approx E_g(\infty) + \frac{c}{L^\delta}, \tag{27}$$

where δ varies between 1 and 1.4 [34–36]. Examples of the reported δ values are 1.16 [37], 1.3 [38], and 1.37 [39]. However, a large power has been observed, such as for undoped ZnO and aluminum-doped ZnO films, and the band gap opening as a function of grain size has been well fitted using $\delta = 1.65$ [40]. From these findings, the general expression for the chemical potential inside an intrinsic semiconductor reads as

$$\mu(L) \approx \mu(\infty)\left(1 + \frac{c/2\mu(\infty)}{L^\delta}\right) + \frac{3}{4}kTln\left(\frac{m_k^*}{m_e^*}\right). \tag{28}$$

This equation also satisfies Equation (17) when choosing $\sigma = \delta$ and $C' \approx c/2\mu_f(\infty)$, and $\phi = 1$. Therefore, we conclude that the general formula can explain all the observed data regarding the effect of size on the chemical potential.

3.2. Size-dependent thermoelectric power

In thermoelectricity, one important parameter related to the conversion figure of merit is the thermoelectric power factor defined as $PF = S^2c$, with S the Seebeck coefficient and c the electrical conductivity of the material. It was predicted by Hicks and Dresselhaus that the thermoelectric power factor increases when the material dimension is decreased [49, 50] and this prediction has challenged many researchers to find the optimal dimension where the conversion is as high as possible. In the last two decades, there were many investigations to deeply understanding how the thermoelectric power changes with material dimension. Both theoretical and experimental investigations have reached the same conclusion that the thermoelectric power changes with material dimension, in accordance with the Hicks and Dresselhaus prediction [49, 50]. However, the final theoretical understanding has not been completely reached. Recently, Hung et al. investigated the quantum size effect on the thermoelectric power of low-dimension materials [51]. They demonstrated theoretically that the thermoelectric power factor increases as $(L/\Lambda)^d/L^3 = \Lambda^d/L^{3-d}$ with L the material dimension, Λ the thermal Broglie wavelength, and d the dimensionality. However, their equation prompts at least one question: the optimum thermoelectric power factor was obtained at $\eta = r+d/2-1$ with r the scattering factor, $\eta = \xi/kT$, where ξ is either $(Ec-\mu)$ or $(\mu - Ev)$ Ec is the bottom of the conduction band and Ev is the top of the valence band. In the calculation, they determined $r = +0.5, r = 0$, and $r = -0.5$ for 1d, 2d, and 3d, respectively, to fit the experimental data. Strangely, by selecting these parameters, it all produced the optimal $\eta = 0$ to mean that the chemical potential was precisely the same as the bottom of the conduction band or the top of the valence band. They compared their prediction with some experimental data from others and there was no evidence that the experimental data were obtained under such conditions $(\eta = 0)$. Based on our finding on the size dependence of chemical potential, we will rederive the size dependence of the thermoelectric power factor with a slightly different approach. We start with the definition of the thermoelectric power factor based on the Mott equation for electrical conductivity and the Seebeck coefficient [52]:

$$c = \int c(E)\left(-\frac{df(E)}{dE}\right)dE \tag{29}$$

and

$$S = -\frac{k}{qc}\int\left(\frac{E-\mu}{kT}\right)c(E)\left(-\frac{df(E)}{dE}\right)dE, \tag{30}$$

where q is the electron charge, $c(E)$ is the energy-dependent electrical conductivity, and f is the Fermi-Dirac distribution function. From this very basic equation, some more detailed formulas for different materials (metals and semiconductors) have been derived. For example, if the equations are applied to semiconductor materials, one obtains

$$S_c = -\frac{k}{e}\left[\frac{E_c-\mu}{kT} + a_c + 1\right], \tag{31}$$

$$\sigma_c = A_c(kT)^{a_c}exp\left[-\frac{E_c-\mu}{kT}\right]\Gamma(a_c+1) \tag{32}$$

for electron transport located at the conduction band. The symbol c refers to the conduction band. Similar equations are applied for holes at the valence band. At present, we focus only on electron transport at the conduction band and assume the hole transport behaves similarly. The parameter a_c originates from the

approximation $c_c(E) = A_c(E - E_c)^{a_c}$ and $\Gamma(x)$ is the gamma function. To obtain the detailed expression for a_c or a_v, let us consider the following derivation. We used the expression for S and c based on relaxation time approximation [53]:

$$S = \frac{1}{qT} \frac{\int v(E)\tau(E)v(E)\left(-\frac{\partial f_0(E)}{\partial(E)}\right)(E-\mu)g(E)dE}{\int v(E)\tau(E)v(E)\left(-\frac{\partial f_0(E)}{\partial E}\right)} g(E)dE, \tag{33}$$

$$c = \int v(E)\tau(E)v(E)\left(-\frac{\partial f(E)}{\partial E}\right)g(E)dE, \tag{34}$$

where $v(E), \tau(E), f(E)$, and $g(E)$ are band carrier velocity, carrier relaxation (scattering) time, the Fermi-Dirac distribution function, and the energy density per unit volume, respectively. By comparing Equations (29) and (34), we conclude that $c(E) = v(E)\tau(E)v(E)g(E)$. Furthermore, we use the following approximations, or $E = d \times (m^* v^2)$ or $v^2(E) = 2E/m^* d$, with d being dimensionality. The relaxation time is assumed to satisfy $\tau(E) = \tau_0 E'$ [54], with τ_0 a constant. Other authors proposed different forms such as $\tau(E) = a_1 E'/(1 + a_2 E')$ with a_1 and a_2 being constants and r a real parameter between 0 and -3 [55] and $g(E) = [D^{3-d} 2^{d-1} \pi^{d/2} \Gamma(d/2)]^{-1} (3m^*/\hbar^2)^{d/2} E^{d/2-1}$. By substituting all those expressions into Equation (34), we obtain

$$c(E) = \frac{2\tau_0}{D^{3-d} m^* d 2^{d-1} \pi^{d/2} \Gamma(d/2)} \left(\frac{3m^*}{\hbar^2}\right)^{d/2} E^{r+d/2}, \tag{35}$$

$$A_c = \frac{2\tau_0}{D^{3-d} m^* d 2^{d-1} \pi^{d/2} \Gamma(d/2)} \left(\frac{3m^*}{\hbar^2}\right)^{d/2}, \tag{36}$$

$$a_c = \frac{d}{2} + r. \tag{37}$$

We have obtained the dependence of the chemical potential on size as shown in Equation (17). We also assume Ec and Ev change similarly with size so that one can write $E_c(E) = E_c(\infty)\chi(D)$ and $E_v(E) = E_v(\infty)\chi(D)$. This is acceptable since when the material dimension changes, the location of energy states changes, including the boundary of conduction and the valence band. Based on this assumption, we can then write

$$E_c(D) - \mu(D) = (E_c(\infty) - \mu(\infty))\chi(D), \tag{38}$$

$$\mu(D) - E_v(D) = (\mu(\infty) - E_v(\infty))\chi(D), \tag{39}$$

and the Seebeck coefficient and the conductivity in Equations (33) and (34) transform into

$$S_c = -\frac{k}{e}[\eta_c \chi(D) + a_c + 1], \tag{40}$$

$$c_c = A_c (kT)^{a_c} exp[-\eta_c \chi(D)]\Gamma(a_c + 1. \tag{41}$$

In Equations (40) and (41), we have introduced new parameters:

$$\eta_c = \frac{E_c(\infty) - \mu(\infty)}{kT}. \tag{42}$$

Using Equations (40)–(42), we obtain the final expression for the thermoelectric power factor and then

$$PF_c = \left(\frac{k}{e}\right)^2 Ac(kT)^{a_c}\Gamma(a_c+1)[\eta_c\chi(D) + a_c + 1]^2 exp[-\eta_c\chi(D)]. \tag{43}$$

Equation (43) is the general expression for size and dimensionality dependence of the thermoelectric power factor. Since $A_c \propto 1/D^{3-d}$ (Equation (36)), we obtain the thermoelectric power factor that changes with size according to $[\eta_c\chi(D) + a_c + 1]^2 exp[-\eta_c\chi(D)]/D^{3-d}$.

Now let us search for the optimum size giving rise to the maximum thermoelectric power factor. We search for the size giving the optimum power factor. The optimum thermoelectric power factor satisfies $dPF_c/dD = 0$. By substituting Ac from Equation (36) into Equation (43), the criterion for the optimum power factor is $d/dD\{[\eta_c\chi(D) + a_c + 1]^2 exp[-\eta_c\chi(D)]/D^{3-d}\} = 0$ to produce

$$-(3-d)[\eta_c\chi(D) + a_c + 1] + \eta_c D(2 - [\eta_c\chi(D) + a_c + 1])\frac{d\chi(D)}{dD} = 0. \tag{44}$$

Equation (44) can be solved if we know the expression for $\chi(D)$. Based on Equation (17), the final expression for $\chi(D)$ depends on $\phi(D)$. For the moment, let us consider a special case of very small size such that $1/D^\sigma >> \phi(D)$. In this case, we can approximate $\chi(D) \approx C'/D^\sigma$ so that Equation (44) can be approximated as

$$-(3-d)\left[\frac{\eta_c C'}{D^\sigma} + a_c + 1\right] - \sigma\left(2 - \left[\frac{\eta_c C'}{D^\sigma} + a_c + 1\right]\right)\left(\frac{\eta_c C'}{D^\sigma}\right) = 0. \tag{45}$$

For the moment, let us also write $y = \eta_c C'/D^\sigma$, and Equation (45) becomes

$$\sigma y^2 + [\sigma(a_c - 1) - (3-d)]y - (3-d)(a_c+1) = 0. \tag{46}$$

The solution for Equation (46) is straightforward, i.e.

$$y = \frac{[\sigma(a_c-1) - (3-d)] + \sqrt{[\sigma(a_c-1) - (3-d)]^2 + 4\sigma(3-d)(a_c+1)}}{2\sigma}$$

or

$$D_{opt} = \left\{\frac{2\sigma\eta_c C'}{[\sigma(a_c-1) - (3-d)] + \sqrt{[\sigma(a_c-1) - (3-d)]^2 + 4\sigma(3-d)(a_c+1)}}\right\}^{1/\sigma}. \tag{47}$$

It is clear that the size of the material that produces the optimum power factor strongly depends on η_c, σ, a_c, and dimensionality. D_{opt} increases linearly with $\eta_c^{1/\sigma}$ and has a complex dependence on σ. The optimum sizes for 0d, 1d, and 2d structures are

$$D_{opt}(0d) = \left\{\frac{2\sigma\eta_c C'}{[\sigma(a_c-1) - 3] + \sqrt{[\sigma(a_c-1) - 3]^2 + 12\sigma(a_c+1)}}\right\}^{1/\sigma}, \tag{48}$$

$$D_{opt}(1d) = \left\{ \frac{2\sigma\eta_c C'}{[\sigma(a_c-1)-2] + \sqrt{[\sigma(a_c-1)-2]^2 + 8\sigma(a_c+1)}} \right\}^{1/\sigma}, \tag{49}$$

and

$$D_{opt}(2d) = \left\{ \frac{2\sigma\eta_c C'}{[\sigma(a_c-1)-1] + \sqrt{[\sigma(a_c-1)-1]^2 + 4\sigma(a_c+1)}} \right\}^{1/\sigma}, \tag{50}$$

respectively. It is clear that if dimensionality increases, the denominators in Equations (48)–(50) decrease, resulting in increases in D_{opt}. Therefore, for a specific material, the thickness of the thin film that produces the optimum power factor is larger than the diameter of nanowires producing the optimum power factor. Now let us estimate the parameter a_c. This parameter determines the optimum power factor. From the parameter a_c, we can then predict the power factor relaxation time, r, based on Equation (37). For $d = 3$, we have

$$D_{opt} = \left\{ \frac{\eta_c C'}{a_c - 1} \right\}^{1/\sigma}. \tag{51}$$

Since the size of 3d material is defined as infinity, the optimum size of 3d material is infinity, too. This leads to the conclusion that $a_c = 1$. Using this value, the optimum sizes for 0d, 1d, and 2d are

$$D_{opt}(0d) = \left\{ \frac{2\sigma\eta_c C'}{-3 + \sqrt{9 + 24\sigma}} \right\}^{1/\sigma}, \tag{52}$$

$$D_{opt}(1d) = \left\{ \frac{2\sigma\eta_c C'}{-2 + \sqrt{4 + 16\sigma}} \right\}^{1/\sigma}, \tag{53}$$

and

$$D_{opt}(2d) = \left\{ \frac{2\sigma\eta_c C'}{-1 + \sqrt{1 + 8\sigma}} \right\}^{1/\sigma}, \tag{54}$$

respectively. Interestingly, we obtain that the optimum size changes are nearly quantized when we move from 0d to 2d.

Let us estimate the optimum sizes as expressed in Equations (52)–(54). If we look back at Equations (24) or (25), we can conclude that C is approximated as $C' \approx 2\hbar^2\pi^2/m_{eff}E_g(\infty)$. For example, for CdS, $E_g(\infty) = 2.42eV, m_e^* = 0.18m_e$ and $m_k^* = 0.53m_e$ [56], so $m_{eff} = 0.134m_e$ and $C' \approx 4.64 \times 10^{-18}m_e$. For CdSe, the reported value is $E_v(\infty) - \mu(\infty) \approx 0.7eV$ eV so that $\eta_c \approx 28$ at room temperature. Using Equations (52)–(54) we obtain the estimated values $D_{eff}(0d) \approx 10.7$ nm, $D_{eff}(1d) \approx 11.4$ nm, and $D_{eff}(0d) \approx 12.9$ nm, respectively.

As explained above, the power factor σ might be different for different materials [34–39]. Therefore, in predicting the optimum sizes that generate the optimum thermoelectric power factor we must first understand the value of σ. As an illustration, in Figure 2 we plot how the optimum diameter changes with σ for 0d, 1d, and 2d materials. In calculations, we use C'$\approx 4.64x0^{-18}m^{\sigma}$ and $\eta_c \approx 28$, i.e. the parameters belong to CdS materials. It is clearly seen that for all dimensions, the optimum diameters increase quickly with the increase of σ, and as the dimension decreases, the optimum diameter is larger at a fixed σ.

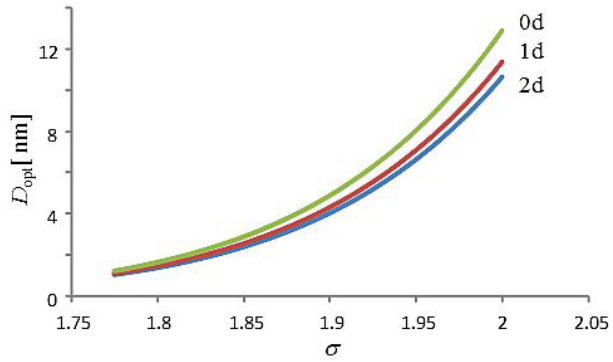

Figure 2. Plot of the optimum diameter change with σ for 0d, 1d, and 2d materials. In calculations, we use C'$\approx 4.64x10^{-18}$ m^{σ} and $\eta_c 28$, i.e. the parameters belong to CdS materials.

Furthermore, using Equation (37) we have the estimation for r as $r = a_c - d/2 = 1 - d/2$. Therefore, for 1d, 2d, and 3d materials we obtain $r = 0.5$, $r = 0$, and $r =$ -0.5, respectively. Those values are precisely the same as used by Hung et al. [51]. The difference is that their values were estimated, while in our work those values occur automatically. The size dependence of the power factor for small sizes can be approximated as

$$PF_c = \Omega(T,d)\frac{\left(\frac{\eta_c C'}{D^{\sigma}} + 2\right)^2 exp\left(-\frac{\eta_c C'}{D^{\sigma}}\right)}{D^{3-d}}, \tag{55}$$

where $\Omega(T,d)$ is a factor that depends on T and d, but is independent of the size. For bulk materials, where $d = 3$ and $D \to \infty$ we have

$$PF_c(\infty) = \Omega(T,3)\frac{\left(\frac{\eta_c C'}{(\infty)^{\sigma}} + 2\right)^2 exp\left(-\frac{\eta_c C'}{(\infty)^{\sigma}}\right)}{1} = 4\Omega(T,3). \tag{56}$$

Hence, the ratio of the optimal power factor to that of the same material in the bulk states becomes

$$\frac{PF_c(D)}{PF_c(\infty)} = \frac{1}{4}\frac{\Omega(T,d)}{\Omega(T,3)} D^{d-3}\left(\frac{\eta_c C'}{D^{\sigma}} + 2\right)^2 exp\left(-\frac{\eta_c C'}{D^{\sigma}}\right). \tag{57}$$

To make the right-hand side of Equation (57) become dimensionless, we must have that $\Omega(T,d)/\Omega(T,3)$ is proportional to $[\text{distance}]^{3-d}$. The common distance quantity that depends on temperature is the de Broglie wavelength. Thus, we suggest $\Omega(T,d)/\Omega(T,3) = (\xi\Lambda)^{3-d}$, with ξ a dimensionless constant. Therefore, Equation (57) should take the following expression:

$$\frac{PF_c(D)}{PF_c(\infty)} = \frac{\xi^{3-d}}{4}\left(\frac{\Lambda}{D}\right)^{3-d}\left(\frac{\eta_c C'}{D^{\sigma}} + 2\right)^2 exp\left(-\frac{\eta_c C'}{D^{\sigma}}\right)$$

$$= \frac{\xi^{3-d}}{4} x^{3-d}\left(\frac{\eta_c C'}{\Lambda^{\sigma}} x^{\sigma} + 2\right)^2 exp\left(-\frac{\eta_c C'}{\Lambda^{\sigma}} x^{\sigma}\right), \tag{58}$$

with $x = \Lambda/D$. This expression is totally different from that of Hung et al., showing that $PF_c(D)/PF_c(\infty) \propto x^{3-d}$ [51].

Figure 3 shows the variation of the thermoelectric power factors for 0d, 1d, and 2d materials when D/Λ changes. In calculations, we use the parameters belonging to CdS: C'$\approx 4.64\times10^{-18}$ m^{σ} and η_c28. In addition, we use $\sigma = 2$ and $\Lambda = 10$ nm. This de Brogile wavelength is similar to that of electrons in silicon at 300 K where the effective mass of electrons is 0.33 me[57] so that $\Lambda = 10.8$ nm.

For all dimensions, the power factors relative to the corresponding values at the bulk states initially increase with size and then decrease as the size gets larger. At very small sizes, the power factor approaches zero. We also identified the presence of the optimal size where the power factors are maximum. The reduction of power factor at very small sizes can be explained in terms of the reduction of electrical conductivity (increase in resistivity) of material at very small sizes. There are several reports on the metal-to-semiconductor transition as the size is reduced [58, 59]. For example, the change of electrical conductivity of metal nanoparticles on size changes similarly to Figure 3 [60]. In Figure 3, we can also observe that at a very small size, the higher power factors belong to materials with lower dimensions. Meanwhile, at larger sizes, the reverse condition occurs, where larger dimension materials have a higher power factor. The thermoelectric power factor of bulk Si is 0.004 W/m K^2 [61]. The power factor of Si NW with a cross-section of 6 nm $\times$ 6 nm was reported as 0.0068 W/m K^2 [62]. This size corresponds to $D/\Lambda \approx 0.56$.

If we compare Equation (58) with Equation (9) in [51], we will notice that

$$\xi^{3-d} = \frac{16vk^2}{qd\Lambda^3}, \tag{59}$$

where v is the carrier mobility. It is then clear that $\xi^{3-d} \propto 1/d$. If we look at Figure 3, at $D/\Lambda \approx 0.56$, the relative power factor for WN (1d) material is around 0.5 in scale of ξ^{3-d}. Therefore, the true power factor must be $3 \times 0.5 = 1.5$-fold of the corresponding value at bulk state. Based on the data reported by Curtin and Boewrs [62], the enhancement of the power factor relative to that in the bulk state is $0.0068/0.004 = 1.7$, very close to our prediction (circle symbol in Figure 3). In addition, Boukai et al. [63] reported that the power factor on SiNW with dimension of 20 nm at 200 K is 0.007 W/m K^2. Since $\Lambda \approx T^{-1/2}$, at this temperature, the de Broglie wavelength becomes 13.2 nm. Therefore, in the report of Boukai et al. [63], we have $D/\Lambda \approx 1.5$. By looking at Figure 3, at this value the relative power factor is also around 0.5 in scale of ξ^{3-d}, or the true enhancement of the power factor relative to that in the bulk state is around 1.5-fold. Again, this prediction is consistent with the experimental data of $0.007/0.004 = 1.75$-fold (triangle symbol). Hochbaum observed a power factor of SiNW with diameter 50 nm at 300 K of as much as 0.00175 W/m K^2 [64]. The enhancement relative to the corresponding value at bulk state was $0.00175/0.004 = 0.4375$. When we put it in Figure 3, this value must be divided by 3 to result in 0.146. The de Broglie wavelength of silicon at 300 K is around 12 nm so for this nanowire we have $d/\Lambda \approx 4.2$. This result is indicated by a square symbol in Figure 3. At small sizes, the power factor increases with the square of temperature, while at large sizes, the power factor decreases with temperature. At a certain size, there is an optimum temperature where the power factor is maximum. The optimum temperature can be derived from Equation (47). In this equation, the temperature occurs in η_c, given by Equation (42). Therefore, for a certain size, the optimum temperature satisfies the following equation:

$$T_c = \frac{1}{kD^{\sigma}}\left\{\frac{2\sigma C'[E_c(\infty)-\mu(\infty)]}{[\sigma(a_c-1)-(3-d)]+\sqrt{[\sigma(a_c-1)-(3-d)]^2+4\sigma(3-d)(a_c+1)}}\right\}. \tag{60}$$

Therefore, for a material of a certain size, one can control the operating temperature to achieve the optimum power factor.

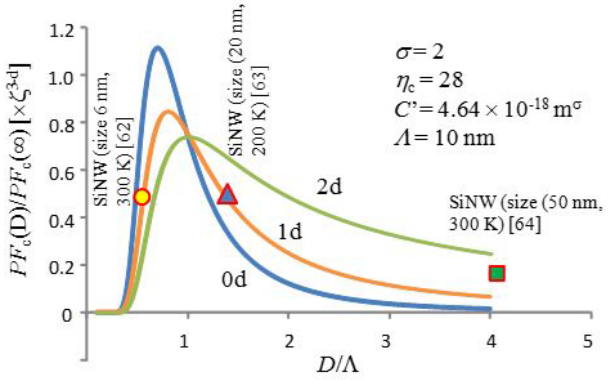

Figure 3. Variation of the thermoelectric power factors for 0d, 1d, and 2d materials when the ratio D/Λ changes. In calculations, we use the parameters belonging to CdS: C'$\approx 4.64 \times 10^{-18} m^{\sigma}$ and $\eta_c 8$. In addition, we use $\sigma = 2$ and $\Lambda = 10nm$. Circle symbol is the experimental power factor of SiNW with cross-section of 6 nm $\times$ 6 nm at 300 K [62], triangle symbol is for the experimental power factor of SiNW with cross-section of 20 nm at 200 K [63], and square symbol is for the experimental power factor of SiNW with cross-section of 50 nm at 300 K [64].

The optimum power factor occurs at different sizes when the de Broglie wavelength changes. For example, Figure 4 shows the plot of the power factor when $\Lambda = 5$ nm. We can observe that materials with higher dimensions have larger power factors at arbitrary sizes than the lower-dimension materials. This figure is different from Figure 3, where the crossover occurs at $D/\Lambda \approx 1$. The locations of optimum power factors are also different from Figure 3, although the optimum sizes for lower dimensions are still smaller than those of higher dimensions.

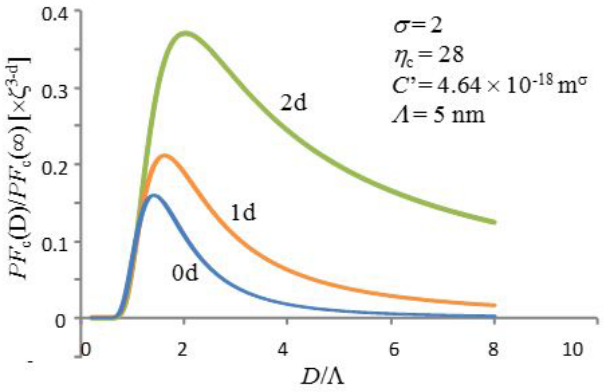

Figure 4. Variation of the thermoelectric power factors for 0d, 1d, and 2d materials when ratio D/Λ changes. In calculations, we use the parameters belonging to CdS: C'$\approx 4.64 \times 10^{-18} m^{\sigma}$ and $\eta_c 8$. In addition, we use $\sigma = 2$ and $\Lambda = 5$ nm.

Finally, we can state that the proposed model has been able to explain the dependence of the thermoelectric power factor on nanostructure size. We showed that the power factor initially increases when reducing the particle size; however, it then approaches zero when further reducing the material size. At very small sizes, the material can change the behavior dramatically. For example, the transition from metal to semiconductor or even to insulator can occur, dramatically reducing the electrical conductivity to imply the loss of carrier

transport ability. We have also tested the model with the experimental data belonging to SiNW both for sizes larger and smaller than the de Broglie wavelength. Both predictions were fairly consistent with the experimental results.

4. Conclusion

We have obtained a general formula for the size dependence of the chemical potential from a very basic formulation, i.e. using the configuration equation as the foundation for deriving the Fermi-Dirac distribution function. The general formula can explain all reports regarding the size dependence of the chemical potential that have been obtained experimentally or theoretically. The chemical potential generally increases with decreasing material dimensions. These properties are very important, since there are many advantageous properties of materials that are controlled by the chemical potential. We have also derived the general equation to describe the size-dependent thermoelectric power factor, which is more general that the equation introduced elsewhere.

Acknowledgment

This work was supported by a research grant from the Ministry of Research and Higher Education of the Republic of Indonesia (No. 1173k/I1.C01/PL/2019) and from Bandung Institute of Technology, Indonesia (No. 91m/I1.C01/PL/2019).

References

[1] Heremans JP, Dresselhaus MS, Bell LE, Morelli DT. When thermoelectrics reached the nanoscale. Nature Nanotechnology 2013; 8 (7): 471. doi: 10.1038/nnano.2013.129

[2] Vining CB. An inconvenient truth about thermoelectrics. Nature Materials 2009; 8 (2): 83. doi: 10.1038/nmat2361

[3] Takeuchi T, Toyama Y, Yamamoto A. Role of temperature dependent chemical potential on thermoelectric power. Materials Transactions 2010; 2010: 1002010989. doi: 10.2320/matertrans

[4] Yamamoto A, Ogawa K, Takeuchi T. Effect of chemical potential on thermoelectric power of Bi_2Te_3 and Bi_2Se_3. Materials Transaction 2011; 2011: 1105301404. doi: 10.2320/matertrans.E-M2011809

[5] Khan B, Yazdani-Kachoei M, Rahnamaye HA, Khan I, Jalali-Asadabadi S et al. Effects of chemical potential on the thermoelectric performance of alkaline-earth based skutterudites (AFe_4Sb_12, ACa, Sr and Ba). Journal of Alloys and Compounds 2017; 6 (94): 253-260. doi: 10.1016/j.jallcom.2016.09.308

[6] Short J, Loo S, Lal S, Hsu KF, Quarez E et al. Hall effect measurements on new thermoelectric materials. In: Materials Research Society Symposium-Proceedings; 2003. pp. 323-332. doi: 10.1557/PROC-793-S8.35

[7] Rhyee JS, Kim Hee J. Chemical potential tuning and enhancement of thermoelectric properties in indium selenides. Materials (Basel) 2015; 8 (3): 1283-1324. doi: 10.3390/ma8031283

[8] Takeuchi T, Otagiri T, Sakagami H, Kondo T, Mizutani U et al. Thermoelectric properties of $Al_8 2.6 - x$ $Re_1 7.4$ Si_x (7 x 12) 1/1-cubic approximants. Physical Review B 2004; 70 (14): 144202. doi:10.1103/PhysRevB.70.144202

[9] Maciá E, Takeuchi T, Otagiri T. Modeling the spectral conductivity of Al-Mn-Si quasicrystalline approximants: a phenomenological approach. Physical Review B 2005; 72 (17): 174208. doi: 10.1103/PhysRevB.72.174208

[10] Kondo T, Takeuchi T, Mizutani U, Yokoya T, Tsuda S et al. Contribution of electronic structure to thermoelectric power in $(Bi, Pb)_2(Sr,La)_2$ CuO_{6+}. Physical Review B 2005; 72 (2): 024533. doi: 10.1103/PhysRevB.72.024533

[11] Takeuchi T, Kaga H, Okada Y, Ikuta H, Baba T et al. Quantitative evaluation of the thermoelectric power of (Bi, Pb) 2 $Sr_2CaCu_2O_{8+}$ from the experimentally determined electronic structure. Journal of Electron Spectroscopy Related Phenomena 2007; 156: 452-456. doi: 10.1016/j.elspec.2006.12.043

[12] Cook G, Dickerson R. Understanding the chemical potential. American Journal of Physics 1995; 63 (8): 737-742. doi: 10.1119/1.17844

[13] Huang ZM, Huang WQ, Wu XK, Liu SR, Qin CJ. Curved surface effect and manipulation of electronic states in nanosilicon. Scientific Reports 2017; 7 (1): 17974. doi: 10.1038/s41598-017-18377-9

[14] Ahmad S, Mukherjee S. A comparative study of electronic properties of bulk MoS2 and its monolayer using DFT technique: application of mechanical strain on MoS2 monolayer. Graphene 2014; 3 (4): 52-59. doi: 10.4236/graphene.2014.34008

[15] Roduner E. Size matters: Why nanomaterials are different. Chemical Society Reviews 2006; 35 (7): 583-592. doi: 10.1039/b502142c

[16] Koole R, Groeneveld E, Vanmaekelbergh D, Meijerink A, de Mello Donegá C. Size effects on semiconductor nanoparticles. Nanoparticles 2004: 13. doi: 10.1007/978-3-662-44823-6_2

[17] Konstantatos G, Sargent EH. Colloidal Quantum Dot Optoelectronics and photovoltaics. Cambridge, UK: Cambridge University Press, 2013. doi: 10.1017/CBO9781139022750.002

[18] Croitoru MD, Shanenko A, Kaun C, Peeters F. Ultra-small metallic grains: effect of statistical fluctuations of the chemical potential on superconducting correlations and vice versa. Journal of Physics Condensed Matter 2012; 24 (7): 275701. doi: 10.1088/0953-8984/24/27/275701

[19] Campbell CT, Mao Z. Chemical potential of metal atoms in supported nanoparticles: dependence upon particle size and support. ACS Catalysis 2017; 7 (12): 8460-8466. doi: 10.1021/acscatal.7b03090

[20] Nagaev EL. Surface forces and chemical potential of small particles. Physica Status Solidi 1991; 167: 381. doi: 10.1021/acscatal.7b03090

[21] Wynblatt P, Gjostein N. Particle growth in model supported metal catalysts—I. Theory. Acta Metallurgica 1976; 24 (12): 1165-1174. doi: 10.1016/0001-6160(76)90034-1

[22] Kiyonaga T, Fujii M, Akita T, Kobayashi H. Size-dependence of fermi energy of gold nanoparticles loaded on titanium (IV) dioxide at photostationary state. Physical Chemistry Chemical Physics 2008; 10 (43): 6553-6561. doi: 10.1039/B809681C

[23] Angus JC, Greber I, Kash K. Size-dependent electron chemical potential: effect on particle charging. Journal of Electrostatics 2013; 71 (6): 1055-1060. doi: 10.1016/j.elstat.2013.10.006

[24] Sodha M, Dubey P. Dependence of fermi energy on size. Journal of Physics D: Applied Physics 1970; 3 (2): 139. doi: 10.1088/0022-3727/3/2/306

[25] Grigor'eva L, Lidorenko N, Nagaev N, Chizhik S. Size dependence of the Fermi energy and of the interaction force between highly disperse particles. Zhurnal Eksperimental'noi i Teoreticheskoi Fiziki 1986; 91 (3): 1050-1062.

[26] Siepmann JI, McDonald I, Frenkel D. Finite-size corrections to the chemical potential. Journal of Physics Condensed Matter 1992; 4 (3): 679. doi: 10.1088/0953-8984/4/3/009

[27] Seitz F. The Modern Theory of Solids. New York, NY, USA: McGraw-Hill Book Company, Inc.; 1940.

[28] Korotun A. Size dependence of the Fermi energy of spherical metal nanocluster. Journal of Nano- and Electronic Physics 2015; 7 (3): 03028.

[29] Seki K. Jellium edge and size effect of chemical potential and surface energy in metal slabs. Journal of the Physical Society of Japan 2018; 87 (12): 124707. doi: 10.7566/JPSJ.87.124707

[30] Turoff RD. Avoiding Stirling's approximation and Lagrange multipliers in introductory statistical mechanics. American Journal of Physics 1970; 38 (3): 387-389. doi: 10.1119/1.1976341

[31] Pointon A. Introduction to Statistical Physics for Students. New York, NY, USA: Longmans; 1967.

[32] Huang K. Statistical Mechanics. New York, NY, USA: John Wiley and Sons; 1987.

[33] Mikrajuddin A. Pengantar Fisika Statistik. Bahasa. Bandung, Indonesia: Rezeki Putra; 2009 (in Indonesian).

[34] Leu PW, Shan B, Cho K. Surface chemical control of the electronic structure of silicon nanowires: density functional calculations. Physics Review B 2006; 73 (19): 195320. doi: 10.1103/PhysRevB.73.195320

[35] Yan JA, Yang L, Chou MY. Size and orientation dependence in the electronic properties of silicon nanowires. Physics Review B 2007; 76 (11): 115319. doi: 10.1103/PhysRevB.76.115319

[36] Yao D, Zhang G, Li B. A universal expression of band gap for silicon nanowires of different cross-section geometries. Nano Letters 2008; 8 (12): 4557-4561. doi: 10.1021/nl802807t

[37] Albe V, Jouanin C, Bertho D. Confinement and shape effects on the optical spectra of small CdSe nanocrystals. Physics Review B 1998; 58: 4713. doi: 10.1103/PhysRevB.58.4713

[38] Mićić OI, Sprague J, Lu Z, Nozik AJ. Highly efficient band-edge emission from InP quantum dots. Applied Physics Letters 1996; 68: 3150. doi: 10.1063/1.115807

[39] Li XD, Chen TP, Liu P, Liu Y, Leong KC. Effects of free electrons and quantum confinement in ultrathin ZnO films: a comparison between undoped and Al-doped ZnO. Optics Express 2013; 21 (12): 14131-14138. doi: 10.1364/OE.21.014131

[40] Fu H, Zunger A. Local-density-derived semiempirical nonlocal pseudopotentials for InP with applications to large quantum dots. Physics Review B 1997; 55 (3): 1642-1653. doi: 10.1103/PhysRevB.55.1642

[41] Singh M, Goyal M, Devlal K. Size and shape effects on the band gap of semiconductor compound nanomaterials. Journal of Taibah University for Science 2018; 12(4): 470-475. doi: 10.1080/16583655.2018.1473946

[42] Patel GR, Thakar NA, Pandya TC. Effect of size on specific heat and Debye temperature of nanomaterials. In: AIP Conference Proceedings; 2016. doi: 10.1063/1.4946189

[43] Zhang Z, Zhao M, Jiang Q. Glass transition thermodynamics of organic nanoparticles. Physica B: Condensed Matter 2001; 293 (3-4): 232-236. doi: 10.1016/S0921-4526(00)00564-0

[44] Xiong S, Qi W, Cheng Y, Huang B, Wang M et al. Universal relation for size dependent thermodynamic properties of metallic nanoparticles. Physical Chemistry Chemical Physics 2011; 13 (22): 10652-10660. doi: 10.1039/c0cp90161j

[45] Kittel C. Introduction to Solid State Physics. 7th ed. New York, NY, USA: John Wiley and Sons; 1996. doi: 10.1119/1.1974177

[46] Brus L. Electronic wave functions in semiconductor clusters: experiment and theory. Journal of Physical Chemistry 1986; 90 (12): 2555-2560. doi: 10.1021/j100403a003

[47] Ferreira DL, Sousa J, Maronesi R, Bettini J, Schiavon, MA et al. Size-dependent bandgap and particle size distribution of colloidal semiconductor nanocrystals. Journal of Chemical Physics 2017; 147 (15): 154102. doi: 10.1063/1.4999093

[48] Takai K, Ikeda M, Yamasaki T, Kaneta C. Size and temperature dependence of the energy gaps in Si, SiC and C quantum dots based on tight-binding molecular dynamics simulations. Journal of Physics Communications 2017; 1 (4): 045010. doi: 10.1088/2399-6528/aa8db4

[49] Hicks L, Dresselhaus MS. Effect of quantum-well structures on the thermoelectric figure of merit. Physical Review B 1993; 47 (19): 12727. doi: 10.1103/PhysRevB.47.12727

[50] Hicks LD, Dresselhaus MS. Thermoelectric figure of merit of a one-dimensional conductor. Physical Review B 1993; 47 (24): 16631-16634. doi: 10.1103/PhysRevB.47.16631

[51] Hung NT, Hasdeo EH, Nugraha AR, Dresselhaus MS, Saito R. Quantum effects in the thermoelectric power factor of low-dimensional semiconductors. Physics Review Letter 2016; 117 (3): 036602. doi: 10.1103/PhysRevLett.117.036602

[52] Cutler M, Mott NF. Observation of Anderson localization in an electron gas. Physical Review 1969; 181 (3): 1336. doi: 10.1103/PhysRev.181.1336

[53] Goldsmid HJ. Introduction to Thermoelectricity. Berlin, Germany: Springer-Verlag; 2010.

[54] Hung NT, Nugraha AR, Hasdeo EH, Dresselhaus MS, Saito R. Diameter dependence of thermoelectric power of semiconducting carbon nanotubes. Physics Review B 2015; 92 (16): 165426. doi: 10.1103/PhysRevB.92.165426

[55] Ahmad S, Mahanti S. Energy and temperature dependence of relaxation time and Wiedemann-Franz law on PbTe. Physics Review B 2010; 81 (16): 165203. doi: 10.1103/PhysRevB.81.165203

[56] Pellegrini G, Mattei G, Mazzoldi P. Finite depth square well model: applicability and limitations. Journal of Applied Physics 2005; 97 (7): 073706. doi: 10.1063/1.1868875

[57] Blatt FJ. Modern Physics. New York, NY, USA: McGraw-Hill College; 1992.

[58] Snow AW, Wohltjen H. Size-induced metal to semiconductor transition in a stabilized gold cluster ensemble. Chemistry of Materials 1998; 10 (4): 947-949. doi: 10.1021/cm970794p

[59] Mobius A, Elefant D, Heinrich A, Muller R, Schumann J et al. The metal-semiconductor transition in amorphous $Si_1 - x Cr_x$ films-scaling behaviour and minimum metallic conductivity. Journal of Physics C: Solid State Physics 1983; 16 (33): 6491. doi: 10.1088/0022-3719/16/33/020

[60] Mikrajuddin A, Shi F, Nieh T, Okuyama K. Metal-to-semiconductor transition in nanocrystals: size and temperature dependence. Microelectronics Journal 2000; 31 (5): 343-351. doi: 10.1016/S0026-2692(99)00144-5

[61] Weber L, Gmelin E. Transport properties of silicon. Applied Physics A 1991; 53 (2): 136-140. doi: 10.1007/BF00323873

[62] Curtin BM, Bowers JE. Thermoelectric power factor enhancement with gate-all-around silicon nanowires. Journal of Applied Physics 2014; 115 (14): 143704. doi: 10.1063/1.4870962

[63] Boukai AI, Bunimovich Y, Tahir-Kheli J, Yu JK, Goddard WA 3rd et al. Silicon nanowires as efficient thermoelectric materials. Nature 2008; 451 (7175): 168-171. doi: 10.1038/nature06458

[64] Hochbaum AI, Chen R, Delgado RD, Liang W, Garnett EC et al. Rough silicon nanowires performance thermoelectric. Nature 2009; 451: 163-168.